Journal of Wind Engineering & Industrial Aerodynamics 275 (2026) 106519

Contents lists available at ScienceDirect

Journal of Wind Engineering & Industrial Aerodynamics

journal homepage: www.elsevier.com/locate/jweia

Modeling vehicle-induced turbulence in large-eddy simulations: Formulation of a simple method and validation against wind tunnel experiments in an idealized street canyon

Giovanna Motisi [a,*], Christof Gromke [b], Matteo Carpentieri [c], Björn Maronga [a]

[a] Leibniz University Hannover, Institute of Meteorology and Climatology, Hannover, Germany
[b] Karlsruhe Institute of Technology, Institute for Water and Environment, Laboratory of Building and Environmental Aerodynamics, Karlsruhe, Germany
[c] University of Surrey, Environmental Flow (EnFlo) Laboratory, School of Engineering, Guildford, UK

ARTICLE INFO

Keywords:
Large-eddy simulation (LES)
Vehicle-induced turbulence (VIT)
Urban street canyon
Pollutant dispersion
Wind-tunnel experiment

ABSTRACT

The transport and dilution of pollutants at street level are dominated by the combined effects of the turbulent background flow and turbulence induced by the motion of vehicular traffic. A thorough understanding of these effects is crucial for the ability to predict the spatial distribution of pollutants correctly. In this study, a new, simple method for modeling vehicle-induced turbulence (VIT) in large-eddy simulations (LESs) of urban street canyon flows is described. The method is validated by comparing results to wind tunnel data of (1) flow around a resting car-shaped body and (2) a street-canyon setup with driving vehicles represented by moving obstacles. The LESs indicate that the main features of the wake flow, including velocity deficit and recirculation length, of a resting car-shaped vehicle is reproduced with good agreement to the experimental data, and shows convergence at a grid spacing of $\Delta = 0.05$ m. In the street-canyon configuration, the simulations capture the primary vortex structure, roof-level separation and associated shear-layer structure, and the associated pollutant dispersion patterns. Moving traffic leads to enhanced vertical exchange and a reduction of in-canyon pollutant concentrations, which is consistently reproduced by the model. A systematic overprediction of streamwise velocity and pollutant removal is observed, suggesting sensitivity to the representation of roof-level momentum exchange. The additional computational cost introduced by the method remains limited (approximately 1%–8%). Overall, these results indicate that the new method provides a simple tool for investigating the influence of moving traffic on urban flow and pollutant dispersion in LES models.

1. Introduction

Traffic emissions are a main contributor to air pollution in urban areas. With the worldwide increase in population as well as the traffic volume in urban environments, the environmental and health impacts of air pollution are of growing concern. Of particular interest is the state of pollution in the urban canopy layer (UCL). Street canyons represent the most basic element in the UCL and have been studied for decades (Oke, 1988; Kastner-Klein and Plate, 1999; Baik and Kim, 1999; Chang and Meroney, 2003; So et al., 2005; Eliasson et al., 2006, among others). They are characterized by high traffic volumes and relatively poor ventilation (Solazzo et al., 2008). These characteristics favor the trapping of exhaust fumes near the surface, especially when coupled to the effects of the building arrangement (Kastner-Klein et al., 2001). Under these conditions, the turbulence generated by the motion of traffic plays a major role in the dilution of pollutants and is therefore critical for urban air quality (Di Sabatino et al., 2003; Solazzo et al., 2007). Nevertheless, the impact of vehicle-induced effects (VIE) on the flow and pollutant dispersion has been investigated only in a limited number of studies. Early field measurements by DePaul and Sheih (1986) indicated that traffic-generated turbulence can significantly modify the vertical structure of the flow, influencing it up to heights of approximately 7 m. In a subsequent study by Qin and Kot (1993) an influence extending up to 12 m above the road surface was reported. Wind tunnel experiments by Kastner-Klein et al. (2001) showed that VIT enhances vertical mixing and reduces pollutant concentrations at street level. This finding was confirmed by further wind tunnel studies (Baker and Hargreaves, 2001; Gromke and Ruck, 2007; Carpentieri et al., 2012), with reported reductions in near-ground concentrations of up to 23% (Ahmad et al., 2002), and by incorporating VIT into Computational Fluid Dynamics (CFD) models.

Existing approaches to represent VIE can be broadly classified according to the representation of vehicles and the underlying turbulence

* Corresponding author.
E-mail address: motisi@meteo.uni-hannover.de (G. Motisi).

https://doi.org/10.1016/j.jweia.2026.106519
Received 27 October 2025; Received in revised form 8 May 2026; Accepted 23 May 2026
Available online 3 June 2026

modeling framework. In the most simplified class, traffic is treated as a continuous forcing, either through boundary-condition-based formulations such as moving wall models (Kim et al., 2016) or through distributed source-term approaches, often referred to as quasi-steady methods, in which momentum and turbulence production are parameterized within the flow field (Jícha et al., 2000, 2002; Sahlodin et al., 2007; Pospisil and Jícha, 2017, 2019). In these approaches, VIT is represented in an averaged sense without explicitly resolving individual wake structure. A second class represents individual vehicles as moving source regions within the domain, for example by introducing localized turbulence or momentum sources associated with each vehicle (Solazzo et al., 2008; Jin et al., 2017). While these approaches account for the spatial and temporal distribution of traffic, they do not explicitly resolve vehicle geometry and therefore cannot reproduce blockage effects or the formation of coherent wake structures.

Higher-fidelity methods explicitly represent vehicles as solid bodies interacting with the flow. These include moving-mesh techniques within RANS frameworks (Li et al., 2017; Wang et al., 2019; Cai et al., 2020) as well as geometry-resolving approaches in LES, such as Eulerian–Lagrangian coupling, multi-fluid formulations, or dynamic overset mesh techniques (Zhang et al., 2017; Woodward et al., 2019; Zhang et al., 2024). While moving-mesh RANS approaches allow for an explicit representation of vehicle motion and mean wake structures, turbulent transport remains fully parameterized, and the associated unsteady wake dynamics are only represented in an averaged sense. As a result, intermittent turbulence production and its interaction with the canyon-scale flow are not resolved.

In urban street canyons, pollutant dispersion results from the interaction between mean-flow structures, such as canyon recirculation, and turbulent mixing processes associated with shear layers and roof-level exchange. As introduced above, RANS models solve equations for time-averaged flow quantities, in which the entire turbulence spectrum is parameterized. Consequently, transient and localized processes associated with vehicle-induced turbulence, are not resolved but instead represented through averaged turbulent fluxes. Consistent with this, Blocken et al. (2008) reported a systematic underestimation of lateral plume spread across a range of commonly used RANS turbulence models, highlighting deficiencies in capturing turbulent mixing and cross-stream transport. This limitation is particularly relevant for street canyon flows, where non-local mixing processes and counter-gradient transport have been reported (Rossi et al., 2010; van Hooff et al., 2014), indicating that turbulent scalar fluxes are not always aligned with local concentration gradients.

In addition, the time-averaging inherent to RANS modeling leads to a strong smoothing of vehicle-induced perturbations. As RANS models rely on temporal averaging over timescales that are much larger than the characteristic turbulence timescales, a moving vehicle is effectively treated as stationary within a RANS averaging interval, i.e., without a physically meaningful relative velocity with respect to the airflow. As a consequence, VIE, which depend on transient wake dynamics and relative motion, cannot be explicitly resolved within this framework. For a street canyon of height $H = 18$ m and an approaching wind speed of $u_{\mathrm{ref}} = 7$ m s^{-1}, a characteristic turnover time of the canyon-scale circulation can be estimated as $H/u_{\mathrm{canyon}} \approx 3.8$ s, assuming $u_{\mathrm{canyon}} = 2/3 \cdot u_{\mathrm{ref}}$ (Oke, 1988). To obtain statistically converged mean quantities, the averaging interval in RANS simulations must be long compared to this timescale. Assuming an averaging interval of 10 s and a vehicle traveling with $u_{\mathrm{veh}} = 11.11$ m s^{-1}, the vehicle travels more than 100 m during this period. As a result, vehicle-induced wake structures and short-lived turbulence production events are averaged over distances several times larger than the canyon height and are therefore strongly smoothed in the mean flow field.

In contrast, LES resolves the dominant, energy-containing turbulent structures explicitly and models only the smaller subgrid-scale motions. This allows the unsteady wake dynamics, intermittent turbulence production, and localized momentum exchange associated with moving vehicles to be captured directly, which is essential for a physically consistent representation of VIT in street canyons.

The first study to investigate VIT by means of LES was performed by Zhang et al. (2017). They followed the Eulerian–Lagrangian approach described by Katolický and Jícha (2005). This method considers moving cars as solid moving Lagrangian "particles" and reproduce the air flow in an Eulerian framework. For each control volume occupied by the vehicle, a drag force is calculated and added as an additional source term to the governing equations. Only grid volumes that are totally occupied by the vehicle are considered. This is, to some extent, problematic because it renders the object effectively permeable to the flow, which may lead to an underrepresentation of blockage effects and wake-induced flow separation. A different approach was adopted by Zheng and Yang (2021, 2022), who applied a quasi-steady formulation within an LES framework. In this method, VIT is introduced as a temporally averaged source term based on the formulation of Katolický and Jícha (2005), such that transient wake structures are not explicitly resolved.

Woodward et al. (2019) employed a multi-fluid method, wherein vehicles are represented as a secondary fluid that displaces the air as they traverse the domain. This approach has been validated against wind tunnel data and can reproduce vehicle-induced flow and dispersion in detail. However, it requires per-vehicle position, speed, and acceleration at each time step, typically obtained from coupled traffic micro-simulations, which adds complexity in setup and data handling.

More recently, Zhang et al. (2024) applied a dynamic overset mesh technique, in which the vehicle geometry is explicitly resolved on a moving grid that overlaps with the background mesh. This approach allows for a detailed representation of vehicle shape and wake dynamics, including flow separation and near-field turbulence structures. However, the method is computationally demanding and requires complex grid generation and interpolation procedures, which may limit its applicability for large-scale or long-duration simulations.

Despite these advances, existing approaches either rely on strong parameterizations of VIT or require computationally expensive, geometry-resolving techniques with additional modeling complexity. Methods based on moving or overset meshes, for instance, involve dynamic grid updates and interpolation between overlapping meshes, which complicates their implementation and increases computational overhead, particularly for simulations with many vehicles or large domains. Similarly, multi-fluid approaches require the transport of additional fields and detailed vehicle trajectory data, often obtained from coupled traffic micro-simulations.

In contrast, the computational cost of LES primarily arises from the need to resolve the relevant turbulent scales, rather than from the vehicle representation itself. This highlights the need for modeling strategies that are compatible with efficient, Cartesian-grid-based LES frameworks and that avoid additional numerical complexity while still capturing the essential physics of VIT.

To provide a simpler and more lightweight alternative compatible with Cartesian grids, we developed a new method to account for VIE in the LES model PALM (Maronga et al., 2015, 2020). The method is capable of representing the explicit shapes of vehicles, but can also be applied to more idealized geometries, such as plates or cuboids, as commonly used in wind tunnel experiments. Validation of the new method is based on two different wind tunnel data sets. In the first setup, a model of a Vauxhall AstraVan was placed in a wind tunnel with zero traveling speed and exposed to a uniform approach flow as described by Carpentieri et al. (2012). This setup allows for a comparison of the wind tunnel data with LES using Cartesian topography for representation of the car as an obstacle as well as the representation of cars with the new method. In the second wind tunnel setup, moving obstacles representing driving vehicles were placed in an idealized street canyon (see Gromke and Ruck, 2007, 2009). In this configuration, the shape of a vehicle and the traffic flow are reduced to a series of plates moving through an idealized street canyon. Together, these two

experiments provide a suitable framework for validating the proposed vehicle representation method.

This paper is structured as follows: in Section 2, the LES model and the formulation of the new method are described, and the experimental and numerical setups are introduced. In Section 3, the results of the validation studies are presented and discussed. Finally, conclusions and an outlook for future work are given in Section 4.

2. Methodology

2.1. Large eddy simulation model

Simulations were conducted using the PALM model system at tagged versions validation_study_1 and validation_study_2.[1] PALM solves the non-hydrostatic, filtered, incompressible Navier–Stokes equations for momentum and scalar quantities on a staggered Cartesian grid in Boussinesq-approximated form. It has been widely used to study various aspects of the urban boundary layer (e.g. Letzel et al., 2012; Gronemeier et al., 2017; Resler et al., 2017; Gronemeier and Sühring, 2019; Kurppa et al., 2020). Discretization in time was achieved by a third-order Runge–Kutta time-stepping scheme (Williamson, 1980) and discretization in space was achieved by the default fifth-order advection scheme in PALM (Wicker and Skamarock, 2002). For the 5th-order advection scheme, the numerical stencil at grid points adjacent to obstacles would require information from within the obstacle. To prevent this, the order of the advection scheme is locally reduced at grid volumes adjacent to obstacles. It is lowered from fifth to third order at the second grid point adjacent to an obstacle, and further reduced from third to first order at grid points directly adjacent to the obstacle surface. We used the 1.5-order turbulence sub-grid scale (SGS) model of Deardoff (1980) in the formulation of Moeng and Wyngaard (1988) and Saiki et al. (2000), which implies an additional equation for the subgrid-scale turbulence kinetic energy. A full overview of PALM is given by Maronga et al. (2015, 2020). The study applies several modules and features embedded in the PALM model system, namely Cartesian topography, self-nesting, and turbulent inflow.

Cartesian topography allows the representation of three-dimensional topologies using the mask method (Briscolini and Santangelo, 1989) with a simplification from Kanda et al. (2004). The mask method uses 3D flag data to mask obstacles and their faces. This allows the code to differentiate between the grid points within, and directly adjacent to, the topography and surrounding atmosphere. With this distinction, additional surface-bounded code (i.e. assumption of a constant-flux layer) is only executed in grid volumes directly adjacent to walls.

Self-nesting allows a domain with a finer resolution to be defined within a larger domain (so-called parent domain). In this study, only one-way nesting is applied, where the finer resolution subdomain (so-called child domain) receives its boundary condition from the coarser resolution parent domain at every time step. For details, see Hellsten et al. (2021).

The turbulent inflow method creates a direct forcing by imposing time-dependent 2D data at a chosen inflow boundary. The boundary data of the prognostic quantities of the velocity components u, v, w and the subgrid-scale turbulent kinetic energy e are generated by a precursor run and processed to a dynamic input file, which is then read by the main run. For details, see Maronga et al. (2020).

[1] The corresponding full commit hashes are 5f9adca36665325c1f9ed5ff7cb523a5f9f54dbd and ff83dc6ab992aeddef7dbc56600174e18cbaca03, respectively.

2.2. Imposed velocity method for representing moving vehicles

The new method implemented in this study (hereafter referred to as Imposed Velocity Method, IVM) prescribes a fixed velocity to the grid volumes representing a moving obstacle (e.g. a vehicle). The imposed velocity corresponds to the prescribed driving speed and direction of the vehicle. In contrast to moving-mesh approaches, the computational grid remains fixed and is not deformed or moved. The vehicle motion is controlled by a marker that tracks the vehicle position in continuous space. At each time step, the marker position is updated according to the prescribed vehicle velocity by adding the product of vehicle speed and time step. The marker is not advected by the resolved flow field, but instead follows the imposed trajectory of the vehicle. Unlike moving-mesh methods, the mesh itself does not follow the vehicle motion. After each update, the three-dimensional mask describing the vehicle geometry is reconstructed within the Eulerian grid. The vehicle geometry itself is defined through a three-dimensional array specifying the occupied grid volumes. The method is compatible with arbitrary terrain representations on the Cartesian grid. The main limitation is that vehicles must move along the grid axes; diagonal motion relative to the grid is currently not supported. The dynamical coupling between the vehicle and the flow field is realized by modifying the momentum tendencies inside the object volumes. Within the occupied grid cells, the velocity tendency is adjusted such that the flow field relaxes towards the prescribed velocity during time integration. Since the subsequent pressure correction does not strictly preserve the imposed velocity inside the obstacle, the prescribed velocity is re-imposed in the occupied grid volumes after the integration step. A schematic overview of the integration procedure is provided in Fig. 1. Since no explicit solid surfaces are represented, surface friction is not considered and no corresponding boundary condition is applied, which again differs from existing moving-mesh approaches. Compared to modifying PALM's Cartesian topography scheme, this approach avoids intrusive changes to the core code structure and remains consistent with the Cartesian grid framework. However, the IVM is different from the treatment of solid obstacles in two aspects. First, surface friction is neglected (no constant flux layer is assumed between air and vehicle). This assumption is based on the fact that for bluff bodies such as road vehicles, aerodynamic drag is dominated by pressure (form) drag, while viscous contributions are comparatively small (Marklund, 2013; White, 2009) (see Section 2.3.1). Second, by imposing the driving speed of the vehicle on the grid volumes, the movement of the vehicle explicitly enters the advection scheme. This is reasonable and more realistic than, e.g., using a constant flux layer, which inherently assumes a zero velocity of the vehicle's surface. The IVM does not require explicit modifications of the SGS model. Instead, the imposed vehicle velocities generate resolved velocity gradients that naturally produce turbulence through the LES dynamics, while the SGS model responds to the resulting strain rates in the same way as for other forcing mechanisms.

2.3. Wind tunnel experiments

2.3.1. Resting vehicle with approaching flow

The experiments involving a car model at rest within a uniform approaching flow were carried out at the EnFlo boundary layer wind tunnel, University of Surrey, UK. It is an open circuit, 'suck-down' wind tunnel with a 20 m × 3.5 m × 1.5 m working section. Reference flow conditions were measured by an ultrasonic anemometer held at a fixed location. Two different geometrical scales for the Vauxhall AstraVan were used (1:5 and 1:20) so that different portions of the wakes could be measured (near and far wakes).

The models were installed approximately 11 m from the inlet of the wind tunnel on a raised false floor in order to position the model above where the boundary layer develops on the wind tunnel floor (see Fig. 2). The dimensions of the false floor were 4150 mm × 90 mm (L × W), with a thickness of 20 mm, placed at a height of 220 mm from

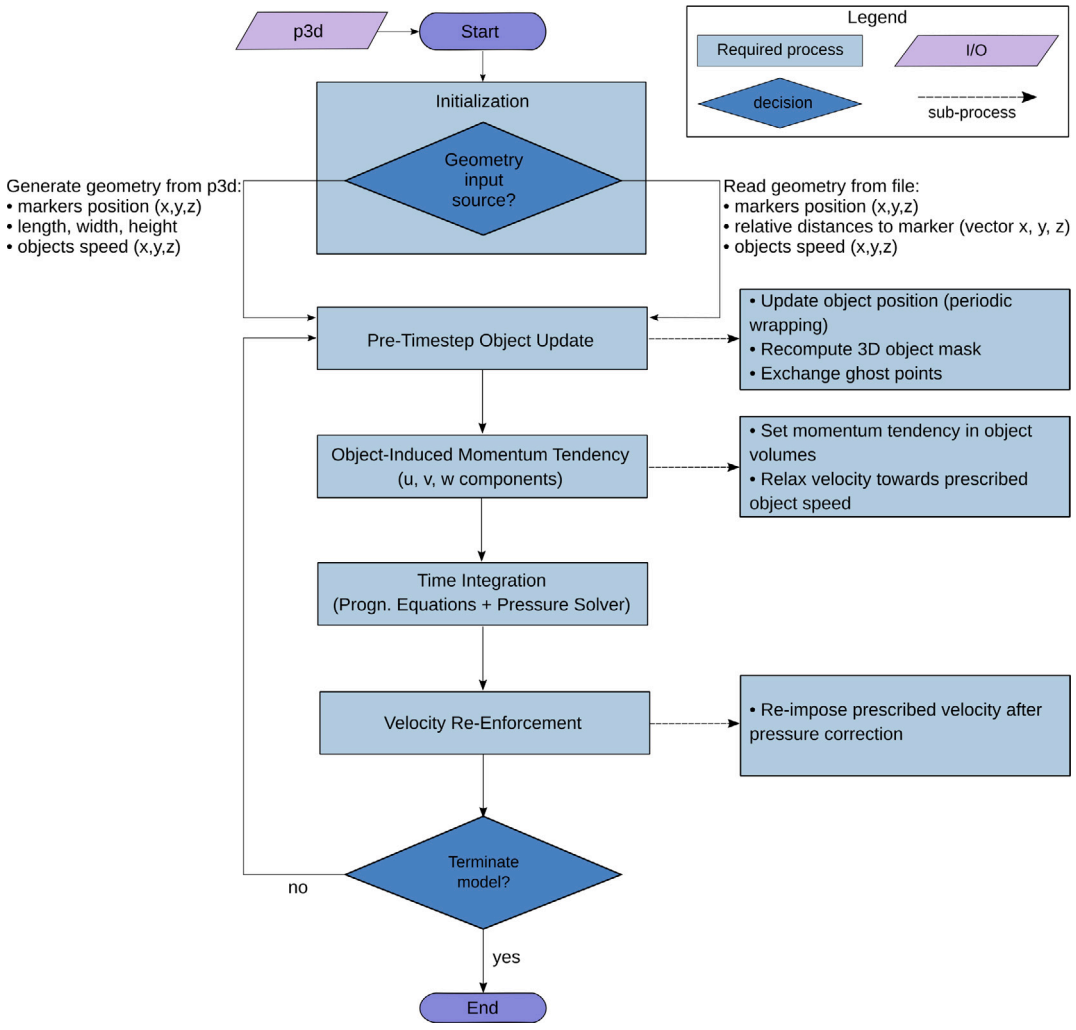

Fig. 1. Flowchart of the numerical time-stepping scheme highlighting the treatment of moving internal objects, including position update, mask reconstruction, object-induced momentum tendencies, and velocity restoration after pressure correction.

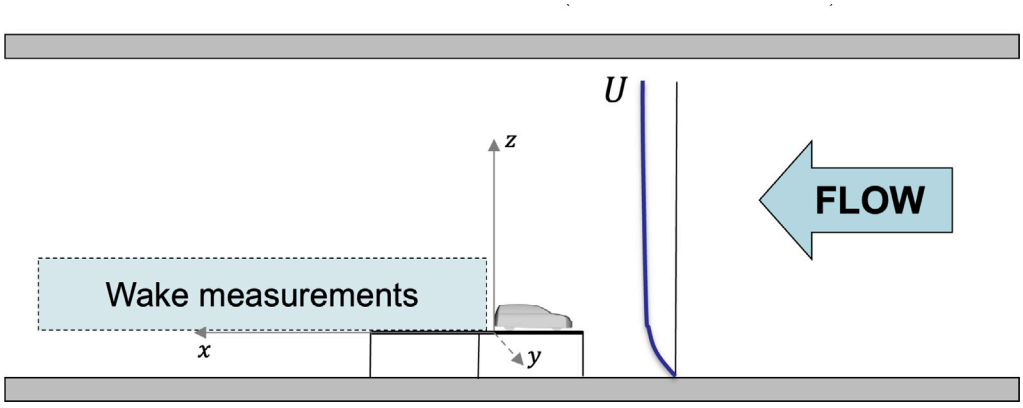

Fig. 2. Schematic representation (not in scale) of the experimental setup in the wind tunnel.

the wind tunnel floor. For reference, the 1:5 model dimensions were approximately: 860 mm × 380 mm × 300 mm, implying a blockage factor of about 2.1%.

A Dantec two-component laser Doppler anemometer (LDA) was used to measure velocity and turbulence fields in the wake of the models at different locations in the wakes of the cars. Tracer concentration measurements using propane gas as tracer and a fast flame ionization detector (FFID) were also conducted but not used in this study. More details about the experiments were described by Carpentieri et al. (2012).

2.3.2. Wind tunnel experiments of street canyon with traffic-induced effects on flow and dispersion

Measurements including the effect of moving traffic on flow and pollutant dispersion in a street canyon were performed in an atmospheric boundary layer wind tunnel at the Laboratory of Building and

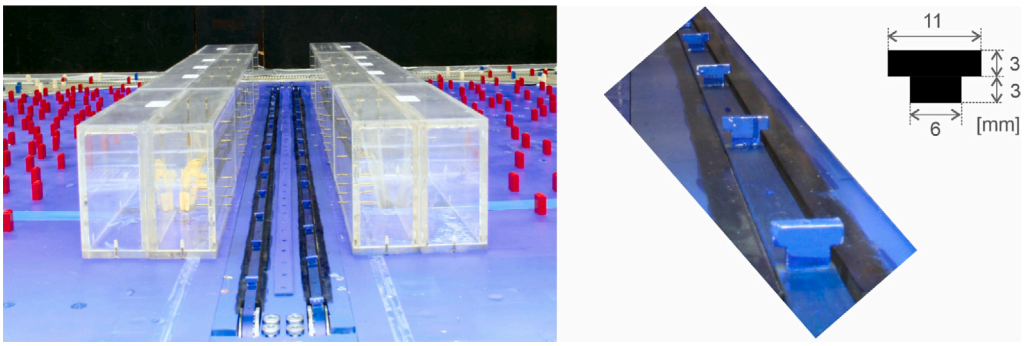

Fig. 3. Model street canyon with traffic belts and close-up of T-shaped plates.

Environmental Aerodynamics at the Karlsruhe Institute of Technology (KIT). The wind tunnel has a cross-section of 2 m by 1 m (width by height) with a test section length of 2 m preceded by a 6 m long flow conditioning section (fetch). Flow conditioning is achieved by means of flow straighteners followed by Irwin-type vortex generators, and a horizontally ground-mounted tripping device. In the fetch and test section, an adjustable ceiling allows to create a flow with zero pressure gradient in streamwise direction. At the location of the test section, an approaching flow is generated which mimics an atmospheric boundary layer whose vertical profiles of the mean streamwise velocity $U(z)$ and streamwise turbulence intensity $I_U(z)$ follow power-law formulations according to

$$\frac{U(z)}{U_{\mathrm{ref}}} = \left(\frac{z}{z_{\mathrm{ref}}}\right)^{\alpha_U} \tag{1}$$

and

$$\frac{I_U(z)}{I_{U,\mathrm{ref}}} = \left(\frac{z}{z_{\mathrm{ref}}}\right)^{\alpha_{I_U}} \tag{2}$$

with z the height above ground, the reference quantities $z_{\mathrm{ref}} = 0.1$ m, $U_{\mathrm{ref}} = 4.39$ m s^{-1}, and $I_{U,\mathrm{ref}} = 22.4\%$ and the profile exponents $\alpha_U = 0.30$ and $\alpha_{I_U} = -0.36$. Based on the profile exponents, the approach flow in the wind tunnel can be considered to be representative of an atmospheric boundary layer typical for urban environments (DIN EN 1991-1-4, 2010; DIN EN 1991-1-4/NA, 2010; VDI 3783-12, 2000). Further information on the characteristics of the simulated atmospheric boundary-layer development (homogeneity) in the streamwise and lateral direction, turbulence intensity $I_U(z)$ and $I_W(z)$, integral length scale $L_{ux}(z)$, and the spectral distribution of turbulence kinetic energy $S_{uu}(z, f)$ - can be found in Gromke and Ruck (2005) and in the CODASC database (CODASC, 2008).

A reduced-scale model (M = 1:150) of a generic street canyon was subjected to perpendicular approach flow in the wind tunnel experiments. The model consisted of two parallel aligned blocks representing rows of houses replicating a full-scale street canyon of street length $L_{\mathrm{S}} = 180$ m and width $W_{\mathrm{S}} = 18$ m bordered by buildings of height $H_B = 18$ m and width $W_B = 18$ m, giving aspect ratios of $L_{\mathrm{S}}/W_{\mathrm{S}} = 10$ and $H_{\mathrm{B}}/W_{\mathrm{S}} = 1$, see Fig. 3. To simulate the release of traffic emissions, four parallel line sources of full-scale length $L_{\mathrm{q}} = 213$ m emitting a tracer gas were installed flush-mounted with the street top according to the principle described in Meroney et al. (1996). The line sources were deliberately chosen to be longer than the street canyon in order to account for traffic emissions released at the sidewise crossings (Gromke and Ruck, 2012). Sampling taps, a total of 98, for concentration measurements were located at the building walls facing the street canyon and realized by cylindrical tubes of outer diameter 2 mm which protrude 5 mm ($x/H = 0.042$) from the wall.

The implication of the motion of vehicles on flow and dispersion within the street canyon was accounted for by plate-shaped bodies mounted on so-called traffic-belts circulating along the street length axis. The assembly consisted of two transmission belts on which thin plates with T-shaped frontal area representing vehicles were affixed at a spacing of 100 mm (see Fig. 3). The transmission belts were embedded in the street floor with only the plates looking out and were separately driven by two electric motors in counter-rotating directions to simulate two-way traffic. It is noted that the traffic belts with the plates were always in place in the model street canyon and were at rest when the effects of moving traffic were not to be considered. The similarity criterion for modeling the effects of moving traffic on flow and dispersion goes back to Plate (1982) and is manifested in the turbulence production ratio TP. The underlying fundamental notion is that the ratio of turbulence production by traffic movement (P_{T}) to turbulence production by the interaction of the approach flow with the urban canopy (P_{U}) shall be equal in full-scale (fs) and reduced-scale (rs), i.e.

$$TP_{\mathrm{fs}} = TP_{\mathrm{rs}} \langle = \rangle \frac{P_{T_{\mathrm{fs}}}}{P_{U_{\mathrm{fs}}}} = \frac{P_{T_{\mathrm{rs}}}}{P_{U_{\mathrm{rs}}}} \tag{3}$$

The turbulence production by traffic movement (P_{T}) within a street canyon of width W_{S} and height H_{B} per unit street length can be estimated as

$$P_{\mathrm{T}} \sim \frac{\rho\, c_{\mathrm{d}}\, u_{\mathrm{T}}^3\, F_{\mathrm{T}}\, n_{\mathrm{T}}}{W_{\mathrm{S}}\, H_{\mathrm{B}}} \tag{4}$$

with ρ the density of air, c_{d} the drag coefficient of vehicles (thin plates), u_{T} the traffic velocity, F_{T} the frontal area of vehicles, and n_{T} the traffic density (vehicles/length). An inherent assumption here is that the complete motion of air induced by traffic movement is transferred to turbulence on a time scale shorter than its residence time in the street canyon. The turbulence production by the interaction of the approach flow with the urban canopy (P_{U}) can be estimated as

$$P_{\mathrm{U}} = \rho\, u_*^2\, \frac{\Delta U}{\Delta z} \sim \frac{\rho\, c_{\mathrm{f}}\, U_\delta^3}{H_{\mathrm{B}}} \tag{5}$$

with u_* the friction velocity, c_{f} the friction coefficient of the urban canopy ($c_f = (\frac{u_*}{U_\delta})^2$), and U_δ the freestream velocity at boundary layer top. Wind tunnel investigations on the validation and suitability of the traffic modeling concept realized by the traffic belts are described in Kastner-Klein and Plate (1999) and Kastner-Klein et al. (2001). In the present study, a scenario involving oncoming traffic at a speed of 40 km h^{-1} and a vehicle density of 6.7 vehicles per 100 m was simulated.

For the dispersion studies, sulphur hexafluoride (SF_6) was used as tracer gas and emitted from the four line sources in the street canyon as described earlier. The air sucked in at the sampling taps at the building walls was analyzed by electron capture detection (ECD), detector type Meltron LH 108, and time-mean concentrations were determined. Velocity measurements at the street canyon top and in front and above the windward building were performed with 2-component laser Doppler velocimetry (LDV) with a commercial system from TSI Incorporated. The LDV data was analyzed for time-mean velocity components.

Table 1
Overview of the grid spacings and resulting dimensions used in the sensitivity study.

Case	Grid spacing ($dx = dy = dz$)	Domain size ($nx \cdot ny \cdot nz$)	Vehicle size ($nx \cdot ny \cdot nz$)
GS1.5	1.5 m	70 × 12 × 14	3 × 1 × 1
GS0.75	0.75 m	140 × 24 × 28	6 × 3 × 2
GS0.5	0.5 m	210 × 36 × 42	9 × 4 × 3
GS0.25	0.25 m	420 × 72 × 84	17 × 8 × 6
GS0.1	0.1 m	1050 × 180 × 210	43 × 19 × 15
GS0.05	0.05 m	2100 × 360 × 420	86 × 38 × 30
GS0.025	0.025 m	4200 × 720 × 840	172 × 76 × 60

2.4. Case description

In both studies, the respective wind tunnel setup was reproduced as accurately as possible. However, this was not possible in all aspects. Both studies were scaled up to reality scale, as already successfully done in other studies (Gronemeier et al., 2021; Zheng and Yang, 2022). Furthermore, cyclic boundary conditions were used in lateral direction, i.e. the domain repeats infinitely in the north-south direction. In the mean flow direction (x-direction), however, non-cyclic boundary conditions were used because using a cyclic condition would have required an extended model domain to allow wake structures to dissipate before re-entering the model domain. At the top, a free-slip boundary condition was applied. Temporal discretization errors are controlled by enforcing a Courant–Friedrichs–Lewy (CFL) number below 0.9, as required by the time-integration scheme of PALM, ensuring numerical stability and a time step that is sufficiently small relative to the resolved turbulent time scales.

2.4.1. Validation study of the IVM for the resting vehicle with approaching flow

In the wind tunnel experiments of Carpentieri et al. (2012) two different model scales were used to investigate both the near wake (1:5 scale) and far wake (1:20 scale) characteristics. The focus of this study was on the near wake, so only the former was used. Scaling to full-scale resulted in a domain size of 100 m by 17.5 m horizontally and 7.5 m vertically. The vehicle size was 4.3 m by 1.9 m horizontally and 1.5 m vertically. To assess the ability of PALM to represent the wake flow of a vehicle with a typical car shape on the Cartesian grid, we performed a sensitivity study in which the grid was successively refined. This allowed us to represent the shape of the car at higher accuracy when decreasing the grid spacing. The sensitivity study started from the coarsest realizable spatial resolution of $\Delta := \Delta x = \Delta y = \Delta z = 1.5$ m (vehicle height) to an extreme high resolution of $\Delta = 0.025$ m (see also Table 1). Due to numerical reasons and internal restrictions the dimensions of the domain were adjusted for the sensitivity study. The adjustments resulted in a domain size of 108 m × 18 m × 22 m (length × width × height). The Vauxhall AstraVan was positioned as closely as possible to the inflow boundary of the model, because it was technically not possible to use a raised floor. This position minimized the surface friction influence on the approaching flow. The largest grid spacing, in this case 1.5 m, was selected uniformly as the distance between the inflow and the vehicle for all grid spacings. A roughness length of $z_0 = 10^{-4}$ m was assumed in order to minimize the effects of surface friction.

The simulation was driven by a horizontal wind speed of 12.5 m s^{-1}, constant with height. In addition, a mass flux correction was applied at the end of each time step to guarantee the conservation of the volume flow. We considered a strictly neutral stratification and neglected the Coriolis force. A constant flux layer was assumed as the surface boundary condition between the bottom and the first computational grid level. At the outflow boundary, the radiation boundary condition was used, which solves the Sommerfeld radiation equation for the velocity components. For scalar quantities, however, a Neumann boundary condition was used.

The total simulation time was 475 s of which the final 400 s were used for data analysis. The first 75 s were omitted from data analysis due to model spin-up effects.

2.4.2. Validation study of the IVM for the moving vehicles in a street canyon under perpendicular flow conditions

For the wind tunnel experiments of Gromke and Ruck (2007), we used a two-domain setup with one-way nesting as described in Section 2 and as shown in Fig. 4, which resulted in a domain size of 290 m by 180 m horizontally and 98 m vertically for the parent domain and 108 m by 180 m horizontally and 50 m vertically for the child domain. The one-way nesting approach was chosen because previous studies have shown that VIT mainly enhances local mixing rather than significantly altering the mean canyon-scale flow (Kastner-Klein et al., 2001; Gromke and Ruck, 2007), which confines it mainly to the street-canyon layer. Consequently, no feedback from the child domain to the parent domain is expected. To assess the influence of grid resolution, we tested three nested domain setups with increasing resolution levels: low (parent 1 m/child 0.5 m), medium (parent 0.5 m/child 0.1 m), and high (parent 0.25 m/child 0.05 m). The nesting approach and overall configuration remained consistent across all resolution levels. The street canyon was represented in both domains, having a height of 18 m, an aspect ratio of 1 and extending over the entire length in the y-direction. Therewith, spatial averaging along the street canyon was possible, which reduced the required simulation time considerably compared to a local time-averaging method as done in the wind tunnel experiments. As a consequence, however, the corner eddies were not represented in PALM (cf. Fig. 3). Analogous to the wind tunnel experiment, the traffic was represented by plates, each plate representing an individual vehicle. For simplicity, the plates were rectangular in shape instead of T-shaped, with respective dimensions of 1.15 m by 0.45 m horizontally and 1.0 m vertically. These dimensions resulted in the same frontal area as the plates used in the wind tunnel experiment. According to the turbulence production similarity criterion described in Section 2.3.2, this simplification does not alter the VIT, provided that the frontal area and drag coefficient are matched to the T-shaped plates used in the wind-tunnel experiments (Plate, 1982; Kastner-Klein and Plate, 1999; Kastner-Klein et al., 2001). The plates were arranged in a two-way traffic scenario with 12 plates per lane and a distance of 15 m between each other. Along each of the four line sources, a surface flux of 1 kg m^{-2} s^{-1} was defined at every grid point. Two traffic scenarios were conducted - a standing traffic case (i.e., vehicles are modeled but do not move) and a two-way traffic case with a speed of 40 km h^{-1}. The small grid spacings and the resulting small time steps of $\Delta t = 0.003$ s for the standing and $\Delta t = 0.001$ s for the moving case led to extremely high computational demands (29 days on 4770 cores). Because further simulations would go beyond the scope of this study, only two traffic scenarios were carried out.

The simulation was initialized via the so-called cyclic-fill method, i.e., the domain was filled repeatedly with 3D data from a (cyclic) precursor simulation and driven by turbulent inflow (Maronga et al., 2015). The setup of the precursor simulation was reduced to 140 m by 180 m horizontally, with the respective grid spacing used for the parent domain in the main run. For initialization of the precursor simulation, we used the approaching wind profile of the wind tunnel experiments with a velocity of 7.02 m s^{-1} at the top of the boundary layer, see Eq. (1). Following Basu and Lacser (2017), a roughness length of at least $z_0 = \frac{1}{50} \cdot min(\Delta z)$ is recommended so that the first grid level is within the inertial sublayer. Due to the staggered grid, the first grid point above the surface is shifted by half the grid width and thus located at $z(1) = 0.5 \cdot \Delta z$. Our first grid point in the parent domain of the highest resolution case is positioned at $z(1) = 0.5 \cdot 0.25 = 0.125$ m, in the child domain at $z(1) = 0.5 \cdot 0.05 = 0.025$ m. With the roughness length of $z_0 = 0.105$ m of the wind tunnel experiments, the recommendation of Basu and Lacser (2017) could hence not be met. Therefore, we explicitly resolved the roughness elements, see Fig. 3, using small blocks

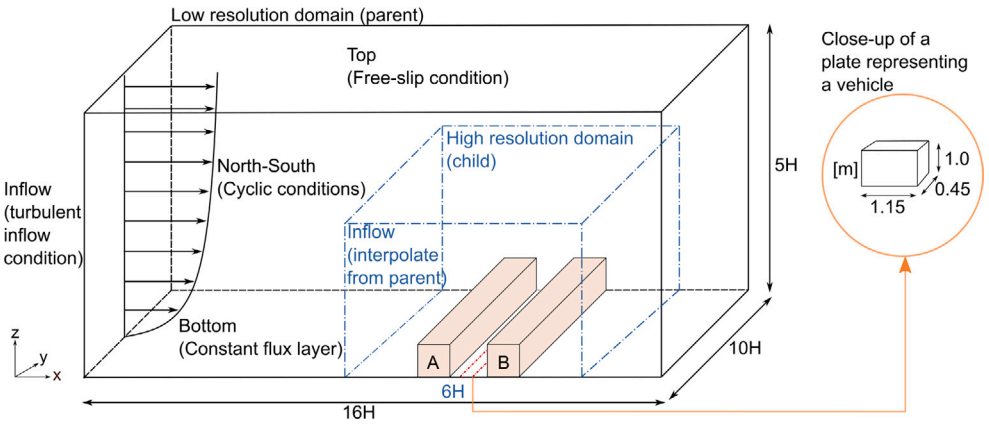

Fig. 4. Schematic of the two-domain LES setup in PALM. The low resolution domain (parent) is shown with a black outline. The nested high resolution domain (child) is highlighted with a blue dashed line. The windward facing building is labeled with A, while the leeward facing building is labeled with B. A close-up of a plate representing a vehicle is outlined in orange. The emission sources are highlighted with red dashed lines.

analogous to those used in the wind tunnel experiments. This approach was applied to all three nested domain setups. For the surface as well as the roughness elements a roughness length of $z_0 = 5{\cdot}10^{-5}$ m was used. This approach was already successfully conducted in Gronemeier et al. (2021).

The precursor run needed 4 h to reach steady state. Inflow data of 500 s were produced for the main run, including 100 s for model spin-up in the main run (flow-through-time) and 400 s for data analysis. The simulation data was then averaged over the full 400 s.

3. Results

3.1. Validation study of the IVM for the resting vehicle with approaching flow

The validation presented here focuses on the representation of the wake of an individual vehicle, which is defined as the region of flow separation at its rear. This occurs due to a sudden change in pressure and results in a velocity deficit that extends many vehicle lengths downstream. The wake is generally divided in two regions: the near wake (closest behind the vehicle) and the far wake (farther behind the vehicle). The near wake usually consists of a re-circulation zone with two counter-rotating vortices and a pair of longitudinal vortices (Ahmed, 1981). The far wake, located downstream the near wake vortices, is an area with increased turbulence but without characteristic coherent structures (Richards, 2003). The extent to which these characteristics were observed in the wind tunnel and in the numerical experiment is discussed below.

Please note that hereafter the topography – both in the wind tunnel and as Cartesian topography in PALM – is considered the reference solution to the problem because it includes the true form and frictional drag forces. Accordingly, a comparison between the wind tunnel data and the LES data of the Cartesian topography is discussed, first. This is followed by a comparison of the wind tunnel data with the IVM.

The measurement points from the wind tunnel experiment are compared in dimensionless form $X = x/h$, $Y = y/h$ and $Z = z/h$, where h is the vehicle height. These points extend from $0.4 \leq X \leq 10.47$ (where the rear of the vehicle is at $X = 0.0$), $-1.33 \leq Y \leq 1.33$ and $0.07 \leq Z \leq 2.0$. Velocities, as well as the root mean square (rms) velocities, have been normalized using the reference wind speed $u_{\mathrm{ref}} = 12.5$ m s^{-1}. Fig. 5 shows the vertical profiles of the dimensionless mean wind speed u/u_{ref} along the vehicle center line for the wind tunnel data (WT) and the LES data of the Cartesian topography. Analogous to the theory explained above, the data of the wind tunnel experiments show a velocity deficit extending over the entire range of the measuring points for the 1:5 scaled model (Fig. 5a). The counter-rotating vortices in the recirculation zone vary in strength and extent. The upper clockwise-rotating flow dominates the zone. The length of the recirculation zone is usually defined as the length between the vehicle base and the stagnation point, where the stagnation point is the local minimum of the local mean velocity $\frac{\bar{u}}{u_{\mathrm{ref}}}$ (Duell and George, 1999). The wind tunnel stagnation point occurs at $X = 1.13$. This is visible in Figs. 5a and 6a. Further downstream of the vehicle, the deficit minimizes continuously (from $2.13 \leq X \leq 7.47$), with negligible changes with height at the furthest measuring point ($X = 10.47$). The simulation data also show a velocity deficit in the direction of flow across all selected grid spacings (see Fig. 5b to h). The counter-rotating vortices in the recirculation zone are both only reproduced with a grid spacing of $\Delta \leq 0.1$ m (see Fig. 5f to h), with the upper one being dominant in strength and extent. Because the first grid point in vertical direction is at $z(1) = 0.5 \cdot \Delta z$, the bottom, counter-clockwise-rotating eddy cannot be explicitly resolved with a coarser resolution. Also, the length of the recirculation zone becomes shorter with increasing resolution and is nearly identical for a grid spacing of $\Delta = 0.05$ m (see Fig. 5g). It is known that the near wake characteristics are highly geometry dependent (Ahmed, 1981, 1983; Morel, 1987; Richards, 2003). Ahmed (1983) for example showed that the recirculation length decreases the larger the rear base slant angle is. Because PALM uses a Cartesian grid, slanted surfaces are difficult to represent and appear as a step-function. The vehicles rear base slant representation is consequently step-like rather than inclined, which could cause the separation to occur at a different location than in the wind tunnel experiment. As the rear becomes "smoother" with higher resolution, the recirculation zone becomes shorter and approaches the lengths observed in the experimental data.

Furthermore, the LES data show that another vortex forms close to the ground for grid spacings less than $\Delta \leq 0.05$ m. This is evidenced by the oscillation of the profiles near the surface (see Fig. 5g and h). Due to the false floor in the wind tunnel experiments, the relative motion between the road and the vehicle is not realistically represented, which results in an build-up of a boundary-layer along the floor (Richards, 2003). The effect is also present in our simulations due to the surface boundary condition and is more pronounced with smaller grid spacings (because these cases effects near the floor cannot be resolved with larger grid spacings). The vortex might thus be a consequence of the developing boundary-layer. Farther downstream of the vehicle, however, the velocity deficit of the wind tunnel data is well represented with a grid spacing of $\Delta = 0.05$ m and $\Delta = 0.025$ m (see Fig. 5g and h). Because of the longer recirculation zone in simulations with grid spacings of $\Delta = 0.25$ m and $\Delta = 0.1$ m, the velocity profiles converge farther downstream. At $x/H = 10.47$, the profiles show, analogous to the experimental data, no significant change over height from a grid spacing of $\Delta = 0.25$ m on.

Fig. 6 shows the vertical profiles of the dimensionless mean speed u/u_{ref} along the vehicle center line for the wind tunnel data and the LES data of the IVM. As the near wake characteristics cannot be properly reproduced with a grid spacing $\Delta \geq 0.1$ m (see discussion above), which is independent of the method used, the results are only shown from a grid spacing of $\Delta = 0.1$ m and lower. The velocity deficit in the streamwise direction is also visible using the IVM method (see Fig. 6b to d). Both counter-rotating vortices in the recirculation zone are reproduced, with the upper vortex exhibiting greater strength and a larger spatial extent than observed in the wind tunnel data. Although the lower vortex in proximity to the vehicle becomes more pronounced as the grid spacing decreases, it is not present away from the vehicle for all grid spacings. It is likely that the differences at the lower edge of the vehicle are due to the missing surfaces. The resulting lack of frictional drag could cause the vortex to separate at a different location (or not at all). As already noted, a different separation location has a direct impact on the wake characteristics (as the roughness influences the production of turbulence). The recirculation zone becomes shorter with decreasing grid spacing and has approximately the same length as in the wind tunnel data for a grid spacing of $\Delta = 0.05$ m and $\Delta = 0.025$ m (see Fig. 6c to d). The LES data of the IVM method also show a change in direction for a grid spacing of $\Delta = 0.025$ m close to the ground (see Fig. 6d), which is also likely due to the surface boundary condition (see discussion above). In the IVM method, the velocity deficit extends beyond the height of the vehicle. The effect is particularly pronounced with a grid spacing of $\Delta = 0.1$ m and $\Delta = 0.05$ m, whereas it does not occur at all with a grid spacing of $\Delta = 0.025$ m. In the case of the first mentioned, a vortex is detached on the vehicle roof, which causes the flow above the vehicle to lift by the vortex' vertical extension. As already mentioned, slanted surfaces are not realized in the present work what makes the representation of the cars step-like rather than inclined, where each individual "step" has the dimension of the grid spacing. Because larger edges cause greater disturbances to the airflow, vortex detachment occurs at grid spacings $\Delta = 0.1$ m and $\Delta = 0.05$ m, but not at $\Delta = 0.025$ m. Beyond $X = 3.8$, the LES profiles—like the wind tunnel data—show little variation with height.

The results of the sensitivity study showed that a grid spacing of at least $\Delta = 0.05$ m is required to reliably reproduce the near wake pattern. This requirement is not directly related to the overall vehicle dimensions, but rather to the need to resolve small-scale flow features in the near wake, such as shear layers, separation regions, and recirculation zones. These features are characterized by much smaller length scales and are highly sensitive to the geometric representation and numerical diffusion, which explains why a comparatively fine grid resolution is necessary. This also agrees with the findings of Letzel et al. (2008), whose resolution study of flow around obstacles in PALM showed that a cube face resolution of 32 grid points is sufficient to achieve convergence of first- and second-order statistics. However, there are some differences in the lower half of the wake (compared to wind tunnel data), which might be related to generally under-resolved flow near solid walls (both bottom surface and vehicle surfaces) or due to the geometry-dependency mentioned above. The magnitude of the streamwise wind component, variance, and wake pattern, however, are generally well produced (the latter two are not shown here). As a compromise between accuracy and computational demands we hence decided to use a grid spacing of 0.05 m for further validation experiments. Consequently, only the simulation data with a grid spacing of $\Delta = 0.05$ m are discussed and presented in the following comparison between the Cartesian topography and the IVM.

Fig. 7 shows the vertical profiles of the dimensionless mean speed u/u_{ref} (left column) and xz–sections of σ_u^2/u_{ref}^2 (right column) along the vehicle center line for the Cartesian topography, the IVM and the wind tunnel data. First of all, a direct comparison of the vertical profiles of the two methods shows that the differences mainly occur in the area close to the vehicle and the ground (see Fig. 7a and b, left). The lower vortex is less pronounced in the case of the IVM which can be recognized by the lower ratio of u/u_{ref} in contrast to the LES data of the Cartesian topography (see Fig. 7a and b, left). Furthermore, the recirculation zone is longer in the case of the IVM, and is located slightly behind $X = 1.13$ for the IVM and slightly in front of $X = 1.13$ for the Cartesian topography. Further downstream of the vehicle (from $X = 2.13$), however, the LES data of both methods show hardly any differences. The streamwise velocity variance in the wind tunnel experiment (see Fig. 7c right) reaches relatively high levels within the recirculation zone, equally peaking at heights corresponding to both the upper and lower edges of the car. This increase in velocity variance can be attributed to shear-induced turbulence, generated from flow separation at the upper and lower edge. These peaks are also visible in the LES data with the upper peak being more pronounced (see Fig. 7a and b right). In the case of the IVM, however, the variance is quantitatively slightly overestimated compared to the Cartesian topography and the wind tunnel data, which indicates that the viscous friction effect of the method might inherently create too much wind shear. At low height levels, the velocity variance is underestimated by the IVM compared to the Cartesian Topography and the wind tunnel data, which can be attributed to the inability of reproducing the flow separation properly at the lower edge, as discussed above.

Table 2
Root Mean Square Error (RMSE) between the LES results with a grid spacing of $\Delta x = 0.05$ m and the wind tunnel data for the normalized streamwise velocity.

Method	Variable	Measuring position	RMSE
IVM	u/u_{ref}	x/h = 0.4	0.609
	u/u_{ref}	x/h = 1.13	0.711
	u/u_{ref}	x/h = 2.13	0.459
	u/u_{ref}	x/h = 3.8	0.227
	u/u_{ref}	x/h = 7.47	0.140
	u/u_{ref}	x/h = 10.47	0.104
Cartesian topography	u/u_{ref}	x/h = 0.4	0.538
	u/u_{ref}	x/h = 1.13	0.449
	u/u_{ref}	x/h = 2.13	0.572
	u/u_{ref}	x/h = 3.8	0.009
	u/u_{ref}	x/h = 7.47	0.009
	u/u_{ref}	x/h = 10.47	0.001

To complement the qualitative analysis of the wake structure, a quantitative comparison between the LES results and the wind tunnel measurements is provided using the root mean square error (RMSE). Table 2 summarizes the RMSE values of the streamwise velocity at different downstream positions along the vehicle center line. The results indicate that the agreement between simulations and experiments improves with increasing downstream distance, consistent with the gradual recovery of the velocity deficit observed in the wake region. In particular, both the Cartesian topography and the IVM show reduced errors for $X \geq 2.13$, where the flow becomes less influenced by near-wake separation effects and more dominated by shear-driven mixing in the far wake. Table 3 summarizes the mean timestep and CPU time per grid point and timestep for each simulation. In this configuration, the additional computational overhead introduced by the IVM is approximately 1%, based on separate performance measurements (not shown here). The computational cost of the IVM is comparable to that of the standard Cartesian topography representation; therefore, only the IVM results are shown.

We conclude that the IVM approach reliably reproduces the general wake structure, including the velocity deficit and shear-induced turbulence farther downstream of the vehicle. It successfully replicates the upper recirculation vortex and the associated peak in velocity variance, which is a key characteristic of wake flows behind bluff bodies. Furthermore, for regions downstream of approximately $X = 2.13$, the IVM shows close agreement with both experimental and high-resolution LES results using the Cartesian topography approach, supporting its suitability for modeling realistic urban traffic scenarios. Nonetheless, two areas for improvement have been identified: (1) the tendency to

Table 3
Mean timestep and CPU time per grid point and timestep. The product of the CPU time per grid point and timestep multiplied by the number of timesteps and the number of grid points in all directions gives the total CPU time.

Case	Δx (m)	$nx \cdot ny \cdot nz$	Δt (s)	# of time-steps	CPU time/grid point and timestep
GS1.5	1.5	70 × 12 × 14	$1.1{\cdot}10^{-1}$	4445	$1.33799{\cdot}10^{-6}$
GS0.75	0.75	140 × 24 × 28	$5.1{\cdot}10^{-2}$	9455	$0.44213{\cdot}10^{-6}$
GS0.5	0.5	210 × 36 × 42	$3.3{\cdot}10^{-2}$	14 600	$0.28067{\cdot}10^{-6}$
GS0.25	0.25	420 × 72 × 84	$1.5{\cdot}10^{-2}$	32 540	$0.01387{\cdot}10^{-6}$
GS0.1	0.1	1050 × 180 × 210	$5.3{\cdot}10^{-3}$	88 795	$0.00255{\cdot}10^{-6}$
GS0.05	0.05	2100 × 360 × 420	$2.5{\cdot}10^{-3}$	193 885	$0.00081{\cdot}10^{-6}$
GS0.025	0.025	4200 × 720 × 840	$1.2{\cdot}10^{-3}$	416 595	$0.00043{\cdot}10^{-6}$

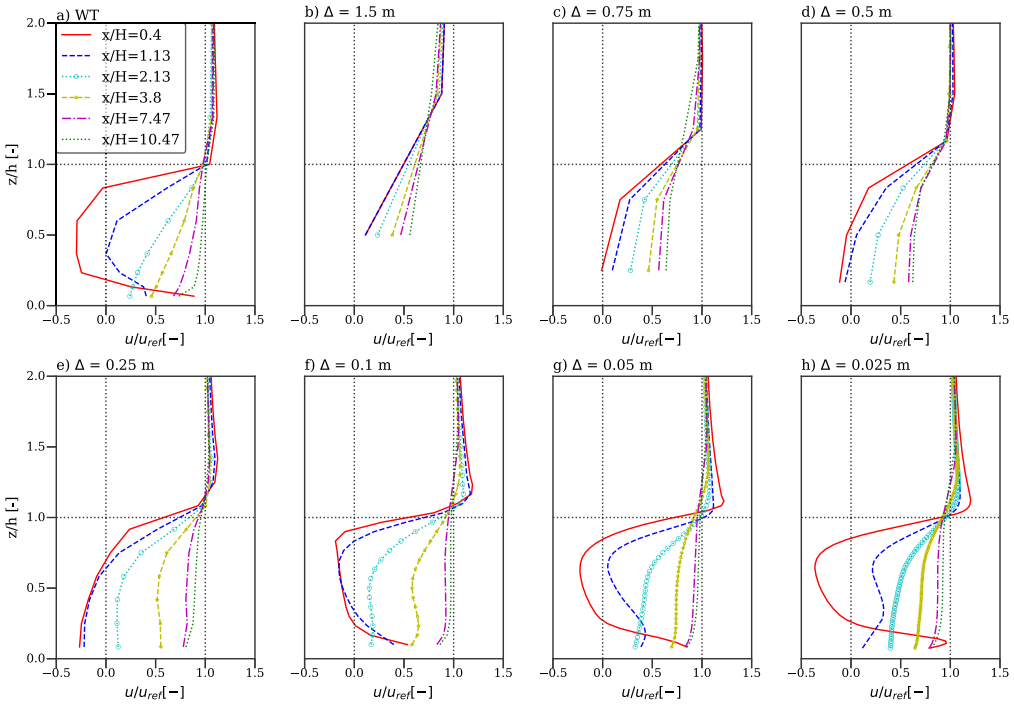

Fig. 5. Vertical profiles of the longitudinal mean speed u/u_{ref} along the vehicle center line for the wind tunnel data (a) and the LES data of the Cartesian topography for the investigated resolutions (b to h). Due to the very low measurement uncertainty in the wind tunnel data (standard error of the mean streamwise velocity below 0.006 m s^{-1} Carpentieri et al., 2012), error bars are omitted in the profile plots as they are not visually resolvable at the scale of the presented figures and would not alter the qualitative or quantitative interpretation. For the LES data, no error bars are shown, as the presented profiles correspond to statistically converged mean quantities.

overestimate velocity variance near the upper edge of the vehicle, likely due to excess shear generation, and (2) the underrepresentation of flow features near the lower vehicle edge and ground, possibly resulting from the absence of frictional surfaces. The latter is likely further enhanced by the Cartesian-grid framework, in which turbulence within the first grid levels above the surface is not fully resolved, resulting in an insufficient representation of the narrow flow region between the vehicle and the ground. While these limitations should be considered, they are relatively minor in the context of urban-scale simulations, where variability in vehicle types, positions, and ambient conditions will dominate wake characteristics. Therefore, we conclude that the IVM is well suited to represent typical vehicle wakes in LES models.

3.2. Validation study of the IVM for the moving vehicles in a street canyon under perpendicular flow conditions

The following evaluation focuses on the flow and dispersion behavior within and above the street canyon, taking into account VIE. In the case of a perpendicular flow and $H/W = 1$, as in the present case, a so-called skimming flow regime develops, resulting in a circulating vortex in the mean flow within the canyon and a mainly undisturbed mean free stream flow above the canyon (Oke, 1988).

The measurement points from the wind tunnel experiment are compared again in dimensionless form $X = x/H$, $Y = y/H$ and $Z = z/H$, where H is the building height. The investigated measurement points extend from $-0.5 \leq X \leq 0.5$ (with $X = 0.0$ being the street canyons center), $Y = 0$ and $1 \leq Z \leq 1.167$ for the velocity data and an extended range of $0.08 \leq Z \leq 0.83$ in front of the canyon walls for the concentration data. Concentrations have been normalized according to

$$c^* = \frac{c_{sim} u_{\mathrm{ref}} H}{Q} \tag{6}$$

with c_{sim} being the simulated concentration [kg m^{-3}], u_{ref} being the free-stream velocity [m s^{-1}] at building height H [m], and Q being the source strength per unit length [kg m^{-1} s^{-1}]. The latter was calculated as

$$Q = \frac{Q'}{L_y} = \frac{\overline{w's'} \cdot 4\Delta \cdot L_y}{L_y} \tag{7}$$

with $\overline{w's'}$ being the flux set in PALM [kg m^{-2} s^{-1}] and L_y being the length of the line sources [m]. In the following, the standing traffic case of the LES data will first be discussed and compared with the wind tunnel data. At the same time we focus only on the child domains of the medium and high resolution setups ($\Delta = 0.1$ m and $\Delta = 0.05$ m), as the

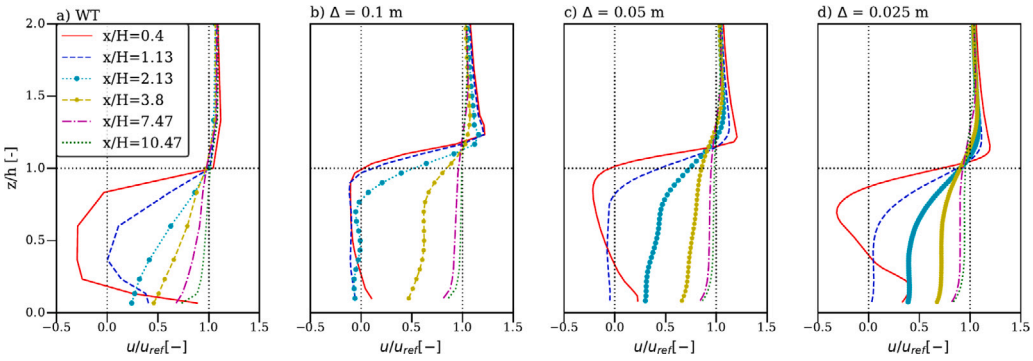

Fig. 6. Vertical profiles of the longitudinal mean speed u/u_{ref} along the vehicle center line for the wind tunnel data (a) and LES data of the IVM for selected resolutions (b to d).

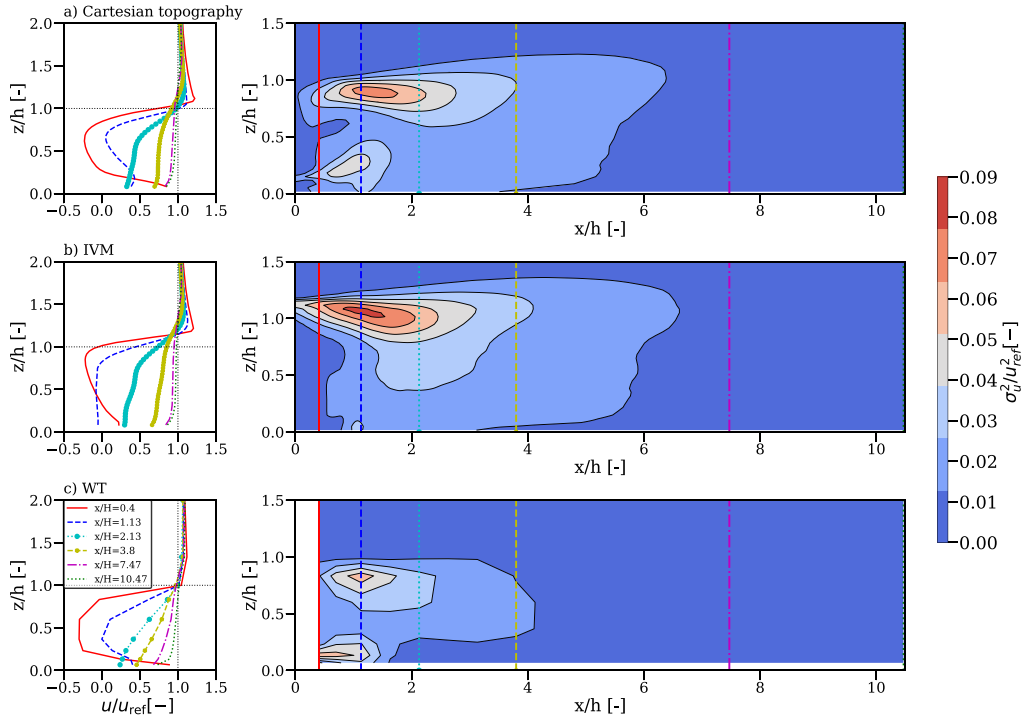

Fig. 7. Vertical profiles of the longitudinal mean speed u/u_{ref} along the vehicle center line for the Cartesian topography (a left), the IVM (b left) and the wind tunnel data (c left) and xz−sections of $\sigma_u^2/u_{\mathrm{ref}}^2$ velocity variance contour plot along the vehicle center line for the Cartesian topography (a right), the IVM (b right) and the wind tunnel data (c right).

cases with a lower resolution were found to be insufficiently resolved to provide meaningful results. Subsequently, the simulation results of the moving traffic case are analyzed and compared both with the wind tunnel data and the data of the standing traffic case. It should be noted that in the wind tunnel experiments, the vertical velocity was measured only above the street canyon for the moving traffic case, whereas for the standing traffic case measurements are available both above and within the street canyon. Therefore, comparisons of in-canyon velocity fields are restricted to the standing traffic case. In contrast to the first validation study, the flow around individual vehicles is not of major concern, only the combined VIE on the pollutant dispersion.

Fig. 8 shows vertical cross sections of the mean vertical velocity component w above the street canyon, along with vertical profiles of the dimensionless concentration c^* within the canyon for the standing traffic case. Both resolutions successfully reproduce the general flow behavior observed in the wind tunnel experiment (see Fig. 8a to b, left). Driven by the mean flow at rooftop, a clockwise-rotating canyon vortex developed between the two walls of the canyon leading to positive values of the vertical velocity w in the upwind half of the canyon ($-0.5 \leq X \leq 0.0$) and to negative values of the vertical velocity w in the downwind half of the canyon ($0.0 \leq X \leq +0.5$). However, one thing is noticeable when comparing the simulation data with the wind tunnel data. The measured wind speeds are somewhat overestimated by the LES data, with the deviation decreasing with increasing resolution. As the vertical up- and downward flow are part of the same circulation system, it is reasonable to assume that a larger amount of the horizontal air flow moves into the street canyon, which in turn causes the vertical flow of the LES data to deviate from the wind tunnel data. The consequence of this is also reflected in the concentration data (see Fig. 8 right). Concentration profiles show higher values at the upwind wall compared to the downwind wall. This accumulation at the upwind wall is caused by the reverse flow close to the street surface, which collects the traffic emissions and transports them towards the upwind wall. The vertical concentration gradients are steeper at the upwind wall, while horizontal gradients dominate near the downwind wall. Both the LES and experimental data exhibit this pattern, which matches the expected behavior in a skimming flow regime (Baik and Kim, 1999; Kastner-Klein and Plate, 1999). Compared to the wind tunnel data, the LES

results tend to underestimate pollutant concentrations at ground level, particularly at the upwind wall. This underestimation is consistent across both resolutions and is more pronounced at finer grid spacings. The likely cause of this underestimation is the slightly stronger vertical exchange in the LES, which enhances pollutant removal from the canyon. This can be attributed to increased vertical velocities driven by stronger inflow at rooftop level. While absolute concentrations differ, the spatial distribution and vertical structure of the LES concentration fields closely resemble those from the wind tunnel.

Fig. 9 shows vertical cross sections of the mean horizontal velocity u around building A and at roof top. The vertical cross sections of the mean horizontal velocity of the wind tunnel data (Fig. 9c) show two characteristic flow phenomena. There is the vortex in front of building A, which emerges due to the deflection of the flow down the windward wall and there is the separation vortex at roof level due to the separation from the sharp edge at the building top. The LES data is able to capture both phenomena (Fig. 9a and b). The intensity and spatial extent of these structures differ to some extent. The LES data show more distinct, compact vortices compared to the wind tunnel data. Additionally, the LES simulations exhibit higher velocities entering the street canyon compared to the wind tunnel, which influences downstream flow patterns and pollutant dispersion. This analysis confirms that the inflow conditions into the canyon are already faster in the LES than in the wind tunnel. This pre-existing overestimation of horizontal wind speeds is consistent with the observations from the standing traffic case and explains why stronger vertical exchange and enhanced pollutant removal occur inside the street canyon.

Fig. 10 shows vertical cross sections of the mean vertical velocity component w above the street canyon and vertical profiles of the dimensionless concentration c^* within the street canyon for the moving traffic case. Compared to the standing traffic case, the vertical velocity fields (see Fig. 10a to c, left) exhibit no significant differences. The VIE seem to be not strong enough to have an influence on the flow field at roof top. In both the experimental data and the LES with fine resolution (see Fig. 10b), the vertical velocities at rooftop level are slightly reduced compared to the standing traffic case. In contrast, the coarser LES resolution (see Fig. 10a) shows a minor increase in vertical velocities. While the flow structure remains largely unchanged, the dispersion behavior within the canyon differs noticeably. In both the wind tunnel and LES data, pollutant concentrations are again higher at the upwind wall than at the downwind wall (see Fig. 10c). The introduction of moving traffic enhances vertical mixing, especially near the upwind wall. In the experimental data, this leads to a significant decrease in concentrations at pedestrian level compared to the standing traffic case (see Fig. 10c, right). The LES results reproduce this trend, but the reduction in concentrations at a grid spacing of $\Delta = 0.1$ m is overly strong compared to the experimental data (see Fig. 10a, right), while the simulation at $\Delta = 0.05$ m provides a more realistic representation (see Fig. 10b, right). These differences can be linked to the variations in rooftop vertical velocities.

To place the present results in a broader modeling context, they are compared with previous RANS- and LES-based street canyon simulations in the following section. A quantitative comparison with existing studies is, however, limited by differences in model configuration and dynamic similarity conditions. While several studies have reproduced the wind tunnel experiments of Gromke and Ruck (2007, 2009), many do not preserve the ratio between the approaching wind speed and the vehicle motion, which is a key parameter governing the resulting flow regime and pollutant dispersion. Among the available literature, Zheng and Yang (2021) provide a unique dataset in which both RANS and LES simulations are performed for a configuration consistent with the experimental setup, including comparable velocity scaling. For this reason, the comparison in the following is primarily focused on their RANS results, while their LES results are used for qualitative context where appropriate. For the streamwise velocity profiles, the RANS standard k-ϵ (SKE) model of Zheng and Yang (2021) reproduces the magnitude of u/u_{ref} at $z/H = 1$ reasonably well, comparable to their LES results (Fig. 10 (a–c) in Zheng and Yang, 2021). However, the vertical gradients are strongly smoothed at higher levels, resulting in an almost linear profile and a reduced ability to capture the gradients observed in the experimental data. In contrast, the present LES results reproduce the mean velocity at $z/H = 1$ with similar accuracy, while additionally capturing a more pronounced vertical structure at higher levels, leading to a non-linear profile. For the vertical velocity component, the RANS model underestimates both the magnitude and vertical variation of w/u_{ref} across all heights. The LES results of Zheng and Yang (2021) show a slight overprediction at the upwind wall and a minor underestimation at the downwind wall (Fig. 10 (d–f) in Zheng and Yang, 2021). In contrast, the present LES results show an overprediction of w/u_{ref} at both walls, while maintaining the overall vertical structure. For the dimensionless concentration c^*, the RANS model shows an overestimation at the upwind and downwind walls, with particularly strong deviations close to the ground. Their LES results show better agreement with the experimental data, especially at the upwind wall where the observed profile is well captured (Fig. 12 (d and k) in Zheng and Yang, 2021). In the present study, concentrations are generally underestimated at both walls, while the overall vertical structure is reproduced well, as discussed above. Overall, the comparison indicates that LES resolves additional flow variability and vertical structure relevant for transport processes, while RANS tends to smooth these features due to its stronger reliance on turbulence parameterization. However, these differences must be interpreted in the context of differing model assumptions and configuration choices. These results underline the importance of resolving unsteady, energy-containing flow structures for an improved representation of vertical exchange processes in street canyon flows.

The deviations in wind speed can be attributed to several uncertainties related to the wind tunnel experiment:

(1) Building roughness: The roughness length of the building surfaces in the wind tunnel experiments is not known. In the numerical model, however, a roughness length of $z_0 = 10^{-3}$ m was used, corresponding to typical values for residential buildings constructed between 1951 and 2000 (Helbig et al., 1999). While the flow field within and around the canyon is primarily governed by the building geometry itself, small differences in surface roughness could still have a minor effect on the turbulence generation and the mean flow above the street canyon.

(2) Resolution and plate positioning: In the wind tunnel experiment, the spatial positioning of the measuring instrumentation can cause that effects may not be detected or inaccuracies may occur due to interpolation. In addition, the position of the plates representing the vehicles in the wind tunnel experiment is not known. The measuring location in the middle of the canyon could thus have been directly adjacent to a plate or not. If the measuring location in the middle of the canyon was located directly above a plate, vertical velocities could be damped as the plate deflects the flow horizontally. If, instead, the measuring location was positioned above a gap between plates, stronger upward motions could occur as the flow is forced to rise around the obstacles. Such localized variations may therefore cause noticeable deviations in the measured wind speed. In the LES, by contrast, these small-scale effects are smoothed out by the spatial averaging along the street canyon.

(3) Corner eddies and domain setup: As mentioned in Section 2.4.2, the street canyon in our simulation domain is infinite. This set-up was chosen on purpose because it allows for spatial averaging along the canyon. Due to the enormous computational costs, it would not have been feasible to collect time series at just the center of the street canyon. As a consequence, however, the air entering the domain can only flow above the canyon but cannot escape to the sides of the buildings, unlike in the wind tunnel experiments. Due to mass conservation, this must result in increased wind speeds above the street canyon. The resulting stronger vertical exchange enhances the pollutant

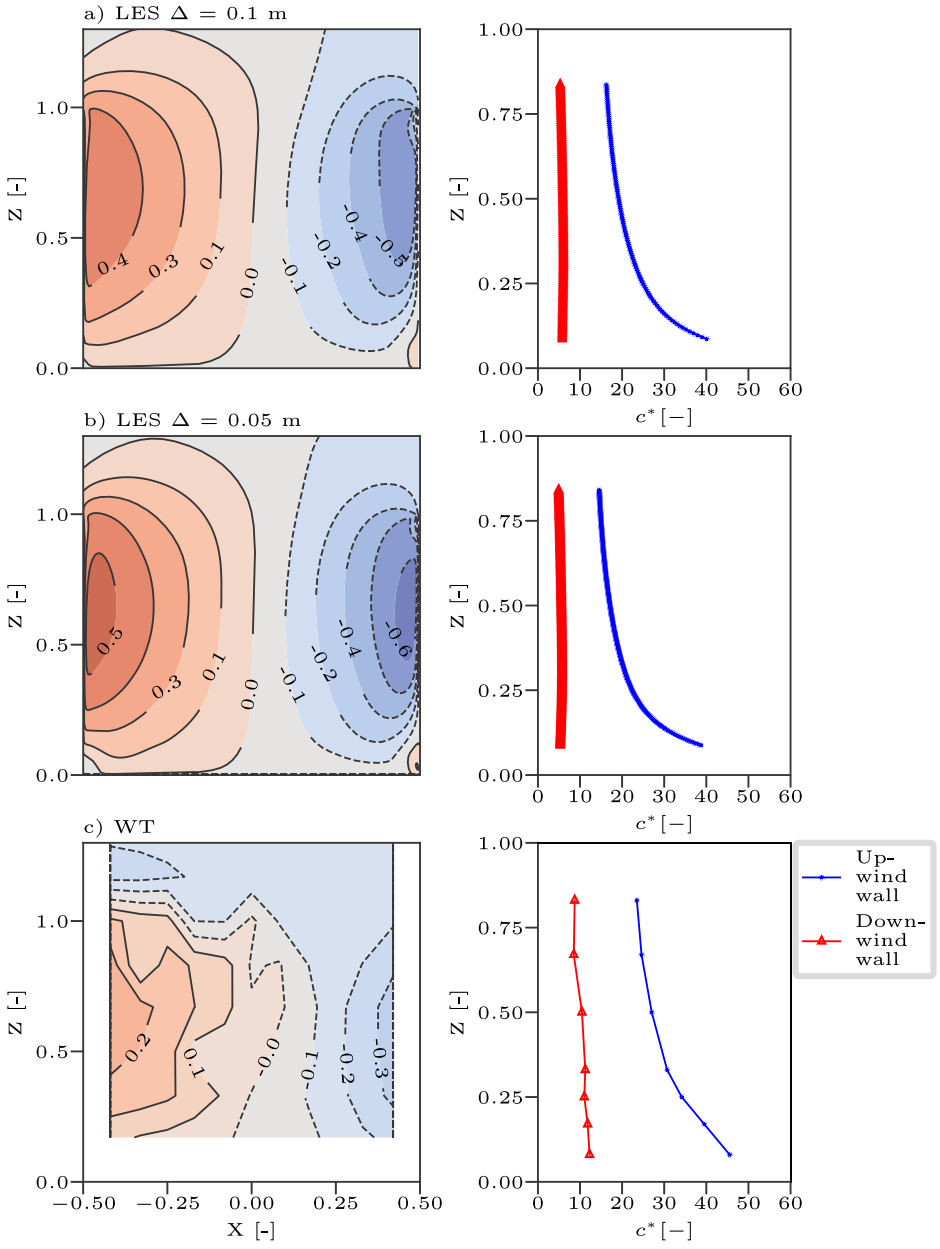

Fig. 8. xz–sections of the mean vertical velocity w [m s^{-1}] within and above the street canyon (left) and vertical profiles of the dimensionless concentration c^* at the upwind and the downwind wall (right) for the LES results for standing traffic with $\Delta = 0.1$ m (a), the LES results with $\Delta = 0.05$ m (b) and the wind tunnel data (c).

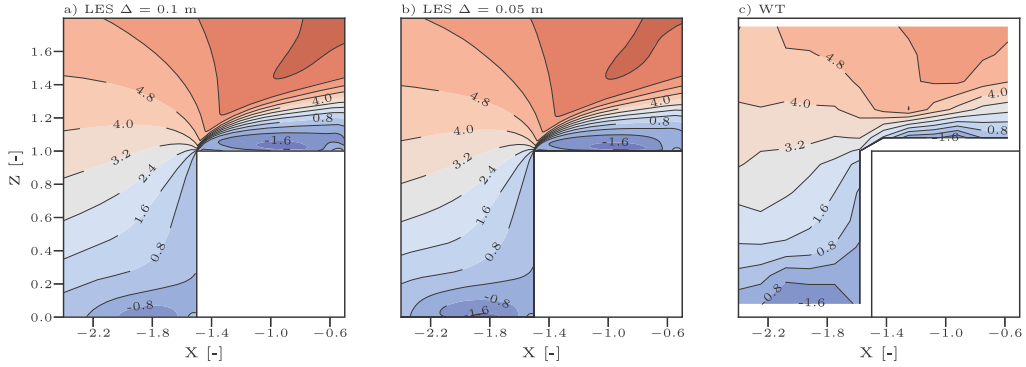

Fig. 9. xz–sections of the mean horizontal velocity u [m s^{-1}] around building A and at roof top for LES results for standing traffic with $\Delta = 0.1$ m (a), the LES results with $\Delta = 0.05$ m (b) and the wind tunnel data (c).

Table 4
Mean timestep and CPU time per grid point and timestep. The product of the CPU time per grid point and timestep multiplied by the number of timesteps and the number of grid points in all directions gives the total CPU time.

Case	Δx (m)	$nx \cdot ny \cdot nz$	Δt (s)	# of time-steps	CPU time/grid point and timestep
Standing traffic	0.5	540 × 900 × 250	$1.5{\cdot}10^{-2}$	31 845	$0.00202{\cdot}10^{-6}$
Standing traffic	0.1	1080 × 1800 × 500	$7.1{\cdot}10^{-3}$	68 751	$0.00094{\cdot}10^{-6}$
Standing traffic	0.05	2160 × 3600 × 1000	$3.2{\cdot}10^{-3}$	153 050	$0.00088{\cdot}10^{-6}$
Moving traffic	0.5	540 × 900 × 250	$1.0{\cdot}10^{-2}$	48 709	$0.00264{\cdot}10^{-6}$
Moving traffic	0.1	1080 × 1800 × 50	$4.2{\cdot}10^{-3}$	115 342	$0.00096{\cdot}10^{-6}$
Moving traffic	0.05	2160 × 3600 × 1000	$1.9{\cdot}10^{-3}$	245 916	$0.00100{\cdot}10^{-6}$

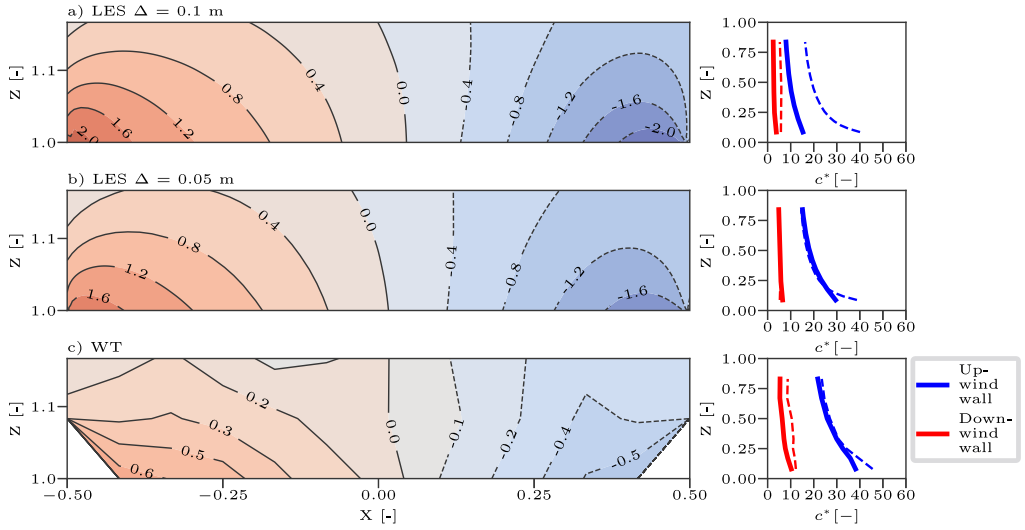

Fig. 10. xz–sections of the mean vertical velocity w [m s^{-1}] above the street canyon (left) and vertical profiles of the dimensionless concentration c^* within the street canyon at the upwind and the downwind wall (right) for LES results for moving traffic with $\Delta = 0.1$ m (a), the LES results with $\Delta = 0.05$ m (b) and the wind tunnel data (c). Dashed concentration profiles correspond to the standing traffic case.

removal, which in turn causes very likely a more pronounced reduction of concentrations within the street canyon than observed in the wind tunnel.

(4) PALM near-wall scalar issue: At the time the simulations were conducted, a previously unknown issue in PALM related to near-wall scalar conservation may have affected the results. This issue has since been identified and resolved, but it may have led to an underestimation of concentrations in the current simulations. Nonetheless, it should be noted that the basic flow characteristics are particularly well captured in the high-resolution domains.

Table 4 summarizes the mean timestep and CPU time per grid point and timestep for each simulation. In this case, the additional computational effort introduced by the IVM is approximately 8%, again based on separate performance measurements (not shown here). The increased overhead compared to the resting-vehicle case is primarily due to the larger number of vehicles represented in the domain, which requires more frequent updates of the imposed velocity field.

We conclude that the general pattern in the wind field as well as the dispersion characteristics is qualitatively well reproduced by the IVM and for both traffic cases, further supporting the validity and applicability of the simulation approach. However, we see that the agreement is better in the moving traffic case than in the standing traffic case, especially for the LES data with a grid size of $\Delta = 0.05$ m. Further studies are planned to test the IVM under different boundary conditions.

4. Conclusion and future work

In this study, a new simple method for modeling VIE in an LES model (here: PALM) was introduced and validated. The newly developed IVM (Imposed Velocity Method) for representing VIT is based on an object, where the vehicles' speed is imposed on the associated grid volumes. Vehicle movement is modeled using a Lagrangian particle that represents the motion of the vehicle's center of gravity, while the shape of the vehicle is represented by a 3D array. The IVM neglects surface friction, reasoning that form drag is the dominant force. The method was validated against experimental data from two different wind tunnel experiments.

In the first setup, a model of a Vauxhall AstraVan was placed in a wind tunnel with zero traveling speed and exposed to a uniform approach flow. It was shown that a grid spacing of at least $\Delta = 0.05$ m is necessary in order to reliably reproduce the near wake pattern. This requirement is not governed by the overall vehicle dimensions, but by the need to resolve small-scale flow features such as shear layers, separation regions, and recirculation zones, which occur on much smaller length scales and are sensitive to both geometric representation and numerical diffusion. Coarser grids lead to a step-like approximation of the geometry, altering separation and distorting the wake. This recommendation follows Letzel et al. (2008), who showed in a resolution study of flow around obstacles in PALM that first- and second-order statistics converge at a cube face resolution of 32 grid points. The overall wake structure, particularly further downstream from the vehicle, was successfully reproduced by the IVM. However, IVM has two limitations: it tends to overestimate vehicle-induced variance at the vehicle's upper edge, and it struggles to capture wake characteristics near the ground close to the vehicle. The latter may be related to the absence of frictional surfaces and is likely enhanced by the Cartesian-grid framework, in which turbulence within the first grid levels are only insufficiently resolved, such that the narrow flow region between the vehicle and the ground is only insufficiently represented. It should be noted, though, that these experiments were designed to represent a specific car type in an undisturbed flow. It can be assumed

that real-world conditions introduce greater variability than the specific limitations observed in the simulation setup.

In the second setup, moving obstacles representing driving vehicles were placed in an idealized street canyon. The comparison of LES simulations and wind tunnel measurements for both standing and moving traffic scenarios shows that the general flow field and dispersion characteristics within an urban street canyon are qualitatively well reproduced by the IVM. Key flow features, such as the canyon vortex and separation vortices at rooftop level, are captured by both LES resolutions, with improved agreement at a grid spacing of $\Delta = 0.05$ m. Nonetheless, LES tends to overpredict horizontal velocities at roof level, which leads to increased pollutant removal from the canyon and consequently lower concentrations compared to the wind tunnel data. These effects are especially pronounced in the LES with $\Delta = 0.1$ m. Despite these discrepancies, the LES qualitatively reproduces the expected dispersion patterns well. Differences can be attributed to several factors, including uncertainties in the wind tunnel setup (e.g., unknown building roughness, vehicle plate positioning, neglected corner eddies), as well as a known issue in PALM related to near-wall scalar conservation, which has since been resolved but may have contributed to an underestimation of concentrations. Despite these limitations, the LES results demonstrate the model's potential to represent key flow and dispersion processes in urban street canyons under conditions comparable to those examined here, in combination with VIE parameterization.

We acknowledge that the present IVM-based LES simulations are computationally expensive compared to RANS-based approaches. However, the objective of this study is not the development of a low-cost predictive tool, but the establishment of a high-fidelity benchmark that explicitly resolves the unsteady flow structures associated with VIT. In this context, the additional computational cost is justified by the ability of LES to capture wake dynamics, localized turbulence production, and their interaction with the canyon-scale flow, which are fully parameterized in RANS approaches. The overall computational effort is primarily governed by the validation-driven setup, in particular the need to preserve wind-tunnel similarity conditions through the imposed combination of high inflow and vehicle velocities, and the corresponding resolution requirements to adequately resolve the resulting flow structures. The use of the nesting approach further contributes to the computational demand. In comparison, the additional cost introduced by the IVM itself is relatively small (about 1% to 8% in the present studies). While the current approach is therefore not yet suitable for large-scale urban applications at city or neighborhood scale, it provides a physically consistent reference for the development and validation of future parameterizations of VIE. In principle, the computational cost could be reduced in future applications through optimization of the nesting strategy (e.g. by disabling timestep synchronization between the parent and child domain) or by using lower absolute velocities while preserving the relevant similarity ratios between wind speed and vehicle speed.

In a follow-up study, we will apply the new IVM to analyze the impact of VIE under heated-surface conditions and for different wind-to-vehicle speed ratios; this paper is already in preparation. A subsequent study will extend the investigation to more complex scenarios, including variations in vehicle fleet composition and geometry, street canyon aspect ratios, roof configurations, wind conditions, and emission source representations. In the longer term, the high-resolution simulations are intended to serve as a basis for deriving simplified parameterizations of VIE that can be applied in coarser-grid LES. The method is generally applicable to LES simulations of moving objects as long as their motion can be represented on the numerical grid; a limitation only arises for processes involving radiative exchange, since the objects are treated as transparent with respect to radiation.

CRediT authorship contribution statement

Giovanna Motisi: Writing – review & editing, Writing – original draft, Visualization, Validation, Software, Methodology, Investigation, Formal analysis, Conceptualization. **Christof Gromke:** Writing – review & editing, Writing – original draft, Validation, Resources. **Matteo Carpentieri:** Writing – review & editing, Writing – original draft, Resources. **Björn Maronga:** Writing – review & editing, Writing – original draft, Validation, Supervision, Project administration, Funding acquisition, Conceptualization.

Declaration of competing interest

The authors declare the following financial interests/personal relationships which may be considered as potential competing interests: Giovanna Motisi reports financial support was provided by German Research Foundation. If there are other authors, they declare that they have no known competing financial interests or personal relationships that could have appeared to influence the work reported in this paper.

Acknowledgments

The author would like to thank Siegfried Raasch (Leibniz University Hannover, Germany) for the valuable scientific comments and discussions. Further thanks go to Christopher Mount (Leibniz University Hannover, Germany) for proofreading. This research has been supported by the Deutsche Forschungsgemeinschaft (DFG, German Reserach Foundation) (grant no. MA 6383/3-1). All simulations were carried out on the computer clusters of the North-German Supercomputing Alliance (NHR). Python 3.10 was used for data analysis and visualization.

Data availability

Data will be made available on request.

References

Ahmad, K., Khare, M., Chaudhry, K., 2002. Model vehicle movement system in wind tunnels for exhaust dispersion studies under various urban street configurations. J. Wind Eng. Ind. Aerodyn. 90, 1051–1064.

Ahmed, S., 1981. An experimental study of the wake structures of typical automobile shapes. J. Wind Eng. Ind. Aerodyn. 9 (1–2), 49–62.

Ahmed, S., 1983. Influence of base slant on the wake structure and drag of road vehicles. J. Fluids Eng. 105 (4), 429—434.

Baik, J., Kim, J., 1999. A numerical study of flow and pollutant dispersion characteristics in urban street canyons. J. Appl. Meteorol. 38 (11), 1576–1589.

Baker, C., Hargreaves, D., 2001. Wind tunnel evaluation of a vehicle pollution dispersion model. J. Wind Eng. Ind. Aerodyn. 89, 187–200.

Basu, S., Lacser, A., 2017. A cautionary note on the use of Monin-Obukhov similarity theory in very high-resolution large-eddy simulations. Bound.-Layer Meteorol. 163, 351–355.

Blocken, B., Stathopoulos, T., Saathoff, P., Wang, X., 2008. Numerical evaluation of pollutant dispersion in the built environment: comparison between models and experiments. J. Wind Eng. Ind. Aerodyn. 93, 1817–1831.

Briscolini, M., Santangelo, P., 1989. Development of the mask method for incompressible unsteady flows. J. Comput. Phys. 85, 57–75.

Cai, C., Ming, T., Fang, W., de Richter, R., Peng, C., 2020. The effect of turbulence induced by differenc kinds of moving vehicles in street canyons. Sustain. Cities Soc. 54, 102015.

Carpentieri, M., Kumar, P., Robins, A., 2012. Wind tunnel measurements for dispersion modelling of vehicle wakes. Atmos. Environ. 62, 9–25.

Chang, C., Meroney, R.N., 2003. Concentration and flow distribution in urban street canyons: wind tunnel and computational data. J. Wind Eng. Ind. Aerodyn. 91, 1141–1154.

CODASC, 2008. Concentration data of street canyons. URL www.codasc.de.

Deardoff, J., 1980. Stratocumulus-capped mixed layers derived from a three-dimensional model. Bound.-Layer Meteorol. 18, 495–527.

DePaul, F., Sheih, C., 1986. Measurements of wind velocities in a street canyon. Atmos. Environ. 20, 445–459.

Di Sabatino, S., Kastner-Klein, P., Berkowicz, R., Britter, R., Fedorovich, E., 2003. The modelling of turbulence from traffic in urban dispersion models – Part I: Theoretical considerations. Environ. Fluid Mech. 3, 129–143.
DIN EN 1991-1-4, 2010. Eurocode 1: Actions on structures – Part 1-4: General actions – Wind actions. Beuth Verlag, Berlin, p. 153.
DIN EN 1991-1-4/NA, 2010. National Annex – Nationally Determined Parameters – Eurocode 1: Actions on Structures - Part 1-4: General actions – Wind actions. Beuth Verlag, Berlin, p. 41.
Duell, E., George, A., 1999. Experimental study of a ground vehicle body unsteady near wake. SAE Trans. 108, 1589–1602.
Eliasson, I., Offerle, B., Grimmond, C., Lindqvist, S., 2006. Wind fields and turbulence statistics in an urban street canyon. Atmos. Environ. 40, 1–16.
Gromke, C., Ruck, B., 2005. Die Simulation atmosphärischer Grenzschichten in Windkanälen. In: Proceedings 13th GALA Fachtagung Lasermethoden in der Strömungsmesstechnik, German Association for Laser Anemometry, Cottbus, Germany. pp. 51.1–51.8.
Gromke, C., Ruck, B., 2007. Influence of trees on the dispersion of pollutants in an urban street canyon - Experimental investigation of the flow and concentration field. Athmospheric Environ. 41, 3287–3302.
Gromke, C., Ruck, B., 2009. Effects of trees on the dilution of vehicle exhaust emissions in urban street canyons. Int. J. Environ. Waste Manag. 4 (1/2), 225–242.
Gromke, C., Ruck, B., 2012. Pollutant concentrations in street canyons of different aspect ratio with avenues of trees for various wind directions. Bound.-Layer Meteorol. 144, 41–64.
Gronemeier, T., Raasch, S., Ng, E., 2017. Effects of unstable stratification on ventilation in Hong Kong. Atmosphere 8 (9), 168.
Gronemeier, T., Sühring, M., 2019. On the effects of lateral openings on courtyard ventilation and pollution - A large-eddy simulation study. Atmosphere 10 (2), 63.
Gronemeier, T., Surm, K., Harms, F., Leitl, B., Maronga, B., Raasch, S., 2021. Evaluation of the dynamic core of the PALM model system 6.0 in a neutrally stratified urban environment: comparison between LES and wind-tunnel experiments. Geosci. Model. Dev. 14 (6), 3317–3333.
Helbig, A., Baumüller, J., Kerschgens, M.J., 1999. Stadtklima und Luftreinhaltung. Springer Berlin, Heidelberg, p. 477.
Hellsten, A., Ketelsen, K., Sühring, M., Auvinen, M., Maronga, B., Knigge, C., Tsegas, F.B.G., Mousslopoulos, N., Raasch, S., 2021. A nested multi-scale system implemented in the large-eddy simulation model PALM model system 6.0. Geosci. Model. Dev. 14, 3185–3214.
van Hooff, T., Blocken, B., Gousseau, P., van Heijst, G., 2014. Counter-gradient diffusion in a slot-ventilated enclosure assessed by LES and RANS. Comput. Fluids 96, 63–75.
Jícha, M., Pospisil, J., 2002. Dispersion of Pollutants in a street canyon and street intersection under traffic-induced flow and turbulence using a low Re k-ϵ model. Int. J. Environ. Pollut. 65 (2), 160–170.
Jícha, M., Pospisil, J., Katolický, J., 2000. Dispersion of pollutants in street canyon under traffic induced flow and turbulence. Environ. Monit. Assess. 18, 343–351.
Jin, X., Yang, L., Du, X., Yang, Y., 2017. Transport charaterstics of PM2.5 inside urban street canyons: The effects of trees and vehicles. Build. Simul. 10, 337–350.
Kanda, M., Moriwaki, R., Kasamatsu, F., 2004. Large eddy simulation of turbulent organized structure within and above explicitly resolved cube arrays. Bound.-Layer Meteorol. 112, 343–368.
Kastner-Klein, P., Fedorovich, E., Rotach, M.W., 2001. A wind tunnel study of organised and turbulent air motions in urban street canyons. J. Wind Eng. Ind. Aerodyn. 89 (9), 849–861.
Kastner-Klein, P., Plate, E., 1999. Wind-tunnel study of concentration fields in street canyons. Atmos. Environ. 33 (24–25), 3973–3979.
Katolický, J., Jícha, M., 2005. Eulerian–Lagrangian model for traffic dynamics and its impact on operational ventilation of road tunnels. J. Wind Eng. Ind. Aerodyn. 93, 61—-77.
Kim, Y., Huang, L., Gong, S., Jia, C., 2016. A new approach to quantifying vehicle induced turublence for complex traffic scenarios. Chin. J. Chem. Eng. 24, 71—-78.
Kurppa, M., Roldin, P., Strömberg, J., Balling, A., Karttunen, S., Kuuluvainen, H., Niemi, J., Pirjola, L., Rönkkö, T., Timonen, H., Hellsten, A., Järvi, L., 2020. Sensitivity study of spatial aerosol particle distribution to the boundary conditions in the PALM model system 6.0. Geosci. Model. Dev. 13 (11), 5663–5685.
Letzel, M., Helmke, C., Ng, E., An, X., Lai, A., Raasch, S., 2012. LES case study on pedestrian level ventilation in two neighbourhoods in Hong Kong. Meteorol. Z. 21 (6), 575–589.
Letzel, M., Krane, M., Raasch, S., 2008. High resolution urban large-eddy simulation studies from street canyon to neighbourhood scale. Atmos. Environ. 42, 8770–8784.
Li, Z., Xu, J., Ming, T., Peng, C., Huang, J., Gong, T., 2017. Numerical simulation on the effect of vehicle movement on pollutant dispersion in urban street. Procedia Eng. 205, 2303–2310.
Marklund, J., 2013. Under-body and Diffuser Flow of Passenger Vehicle (Ph.D. thesis). Chalmers University of Technology, SE.
Maronga, B., Banzhaf, S., Burmeister, C., Esch, T., Forkel, R., Fröhlich, D., Fuka, V., Gehrke, K.F., Geletič, J., Giersch, S., Gronemeier, T., Groß, G., Heldens, W., Hellsten, A., Hoffmann, F., Inagaki, A., Kadasch, E., Kanani-Sühring, F., Ketelsen, K., Khan, B.A., Knigge, C., Knoop, H., Krč, P., Kurppa, M., Maamari, H., Matzarakis, A., Mauder, M., Pallasch, M., Pavlik, D., Pfafferott, J., Resler, J., Rissmann, S., Russo, E., Salim, M., Schrempf, M., Schwenkel, J., Seckmeyer, G., Schubert, S., Sühring, M., von Tils, R., Vollmer, L., Ward, S., Witha, B., Wurps, H., Zeidler, J., Raasch, S., 2020. Overview of the PALM model system 6.0. Geosci. Model. Dev. 13 (3), 1335–1372.
Maronga, B., Gryschka, M., Heinze, R., Hoffmann, F., Kanani-Sühring, F., Keck, M., Ketelsen, K., Letzel, M.O., Sühring, M., Raasch, S., 2015. The parallelized Large-Eddy simulation model (PALM) version 4.0 for atmospheric and oceanic flows: model formulation, recent developments, and future perspectives. Geosci. Model. Dev. 8 (8), 2515–2551.
Meroney, R., Pavageau, M., Rafailidis, S., Schatzmann, M., 1996. Study of line source characteristics for 2-D physical modelling of pollutant dispersion in street canyons. J. Wind Eng. Ind. Aerodyn. 62, 279–290.
Moeng, C., Wyngaard, J., 1988. Spectral analysis of Large-Eddy simulations of the convective boundary layer. J. Atmos. Sci. 45, 3573–3587.
Morel, T., 1987. The Effect of Base Slant on the Flow Pattern and Drag of Three-Dimensional Bodies with Blunt Ends. Springer US.
Oke, T., 1988. Street design and urban canopy layer climate. Energy Buil 11 (1), 103–113. http://dx.doi.org/10.1016/0378-7788(88)90026-6.
Plate, E., 1982. Windkanalmodellierung von Ausbreitungsvorgängen in Stadtgebieten. In: Abgasbelastungen durch den Kraftfahrzeugverkehr. Verlag TÜV Rheinland GmbH, pp. 61–83.
Pospisil, J., Jícha, M., 2017. Influence of vehicle-induced turbulence on pollutant dispersion in street canyon and adjacent urban area. Int. J. Environ. Pollut. 62, 89–101.
Pospisil, J., Jícha, M., 2019. Numerical modelling of transient dispersion of air pollution in perpendicular urban street intersection with detail inclusion of traffic dynamics. Int. J. Environ. Pollut. 65, 71–83.
Qin, Y., Kot, S., 1993. Dispersion of vehicular emission in street canyons, Guangzhou City, South China (P.R.C.). Atmos. Environ. 27B, 283–291.
Resler, J., Krč, P., Belda, M., Juruš, P., Benešová, N., Lopata, J., Vlček, O., Damašková, D., Eben, K., Derbek, P., Maronga, B., Kanani-Suehring, F., 2017. PALM-USM v1.0: A new urban surface model integrated into the PALM large-eddy simulation model. Geosci. Model. Dev. 10 (10), 3635—-3659.
Richards, K., 2003. Computational modelling of pollution dispersion in the near wake of a vehicle (Ph.D. thesis). University of Nottingham, UK.
Rossi, R., Philips, D., Iaccarino, G., 2010. A numerical study of scalar dispersion downstream of a wall-mounted cube using direct simulations and algeabric flux models. Int. J. Heat Fluid Flow 31, 805—-819.
Sahlodin, A., Sotudeh-Gharebagh, R., Zhu, Y., 2007. Modeling of dispersion near roadways based on the vehicle-induced turbulence concept. Atmos. Environ. 41, 92–102.
Saiki, E., Moeng, C., Sullivan, P., 2000. Large-Eddy simulation of the stably stratified planetary boundary layer. Bound.-Layer Meteorol. 95, 1–30.
So, E.S.P., Chan, A.T.Y., Wong, A.Y.T., 2005. Large-eddy simulations of wind flow and pollutant dispersion in a street canyon. Atmos. Environ. 39 (20), 3573–3582.
Solazzo, E., Cai, X., Vardoulakis, S., 2008. Modelling wind flow and vehicle-induced turbulence in urban streets. Atmos. Environ. 42 (20), 4918–4931.
Solazzo, E., Vardoulakis, S., Cai, X., 2007. Evaluation of traffic-producing turbulence schemes within operational street pollution models using roadside measurements. Atmos. Environ. 41 (26), 5357–5370.
VDI 3783-12, 2000. Environmental Meteorology – Physical Modelling of Flow and Dispersion Processes in the Atmospheric Boundary Layer – Applications of Wind Tunnels. Beuth Verlag, Berlin, p. 36.
Wang, Q., Fang, W., et al., 2019. Effect of moving vehicles on pollutant dispersion in street canyon by using dynamic mesh updating method. J. Wind Eng. Ind. Aerodyn. 187, 15–25.
White, F., 2009. Fluid Mechanics. McGraw-Hill.
Wicker, L., Skamarock, W., 2002. Time-splitting methods for elastic models using forward time schemes. Mon. Weather Rev. 130 (8), 2088–2097.
Williamson, J., 1980. Low-storage Runge-Kutta schemes. J. Comput. Phys. 35 (1), 48–56.
Woodward, H., Stettler, M., Pavlidis, D., Aristodemou, E., ApSimon, H., Pain, C., 2019. A large eddy simulation of the dispersion of traffic emissions by moving vehicles at an intersection. Atmoshperic Environ. 215, 116891.
Zhang, Y., Gu, Z., Yu, C.W., 2017. Large eddy simulation of vehicle induced turbulence in an urban street canyon with a new dynamically vehicle-tracking scheme. Aerosol Air Qual. Res. 17, 865–874.
Zhang, Y., Wen, L., Zhang, X., Fu, Y., Tse, T., Mak, C., 2024. Enhanced modeling of vehicle-induced turbulence and pollutant dispersion in urban street canyon: Large-eddy simulation via dynamic overset mesh approach. Sustain. Cities Soc. 117, 105939.
Zheng, X., Yang, J., 2021. CFD simulations of wind flow and pollutant dispersion in a street canyon with traffic flow: Comparison between RANS and LES. Sustain. Cities Soc. 75, 103307.
Zheng, X., Yang, J., 2022. Impact of moving traffic on pollutant transport in street canyons under perpendicular winds: A CFD analysis using large-eddy simulations. Sustain. Cities Soc. 82, 103911.